



Bulk QCD Thermodynamics and Sterile Neutrino Dark Matter

Kevork N. Abazajian*

NASA/Fermilab Astrophysics Group, Fermi National Accelerator Laboratory, Box 500, Batavia, Illinois 60510-0500

George M. Fuller†

Department of Physics, University of California, San Diego, La Jolla, California 92093-0319

(Dated: April 17, 2002)

We point out that the relic densities of singlet (sterile) neutrinos of interest in viable warm and cold dark matter scenarios depend on the characteristics of the QCD transition in the early universe. In the most promising of these dark matter scenarios the production of the singlets occurs at or near the QCD transition. Since production of the singlets, their dilution, and the disappearance of weak scatterers occur simultaneously, we calculate these processes contemporaneously to obtain accurate predictions of relic sterile neutrino mass density. Therefore, a determination of the mass and super-weak mixing of the singlet neutrino through, for example, its radiative decay, along with a determination of its contribution to the critical density can provide insight into the finite-temperature QCD transition.

PACS numbers: 95.35.+d,14.60.St,12.38.Mh,25.75.-q

FERMILAB-Pub-02/067-A

I. INTRODUCTION

In this paper we show how the temperature and the order (first order or not) of the QCD transition in the early universe is important in determining the relic densities of sterile neutrinos in models where they provide the dark matter. The QCD transition epoch is the regime where the quark and gluon degrees of freedom annihilate, chiral symmetry is broken, and quarks are incorporated into color singlets. For the low chemical potential (i.e., small baryon number or high-entropy) characterizing the universe, we expect the QCD epoch to occur at a temperature (energy scale) of order the pion mass, $T_{\text{crit}} \sim 100$ MeV. Coincidentally, this is the temperature regime where the dark matter singlet neutrinos are produced by scattering-related processes.

Therefore, an accurate calculation of the density of dark matter candidate sterile neutrinos requires detailed specification of the evolution of the background plasma through the QCD transition. It is conceivable that this relation between the QCD transition and sterile neutrino properties could be exploited to understand the cosmic QCD epoch. This approach is not available, for example, with supersymmetric dark matter candidates which freeze-out of the plasma at temperatures well above the QCD transition. Here, we also review the current best constraints on sterile neutrino dark matter candidates.

The current cosmological paradigm of a spatially flat Friedmann-Lemaitre-Robertson-Walker (FLRW) universe with critical density components shared between

cold dark matter (CDM, $\Omega_m \sim 0.3$) and a negative-pressure dark energy ($\Omega_X \sim 0.7$), with nearly scale-invariant adiabatic Gaussian perturbations produced by inflation leading to structure formation (Λ CDM), is supported by a concordance of observational evidence from the cosmic microwave background, large scale structure, rich galaxy clusters, and high-redshift Type-Ia supernovae [1]. There is much optimism in observational cosmology, but a number of unresolved problems remain. Among them is the very nature of particle dark matter and dark energy.

More astrophysically, there may be a discrepancy between the quantity of substructure on galactic scales predicted in numerical simulations using Λ CDM initial conditions and that observed in the local group: the “dwarf-galaxy problem” [2, 3]. Another discrepancy exists between the observed flat and low density profiles of dwarf galaxy cores [4, 5] relative to those found in N -body simulations. One solution to the dwarf-galaxy problem is a modification of the primordial power spectrum at sub-galaxy scales by thermal damping of perturbations by warm dark matter (WDM) [6]. Dwarf-galaxy halos in WDM scenarios form through fragmentation of larger structures, and the concentrations of their halos may be reduced [8]. Although these problems may be signaling the presence of WDM, the apparent dwarf-galaxy problem may be the result of dispersion of baryons from halos due to late reionization or supernovae, so that the unobserved dwarf halos are simply dark. These issues could be resolved through refined calculations of star formation in small halos, or through observations of galactic substructure in, for example, gravitational lensing studies [7].

Sterile neutrinos are a natural candidate for WDM [9, 10] and CDM [11, 12], and can emerge from models with composite fermions [13], mirror fermions [14] or light axi-

*Electronic address: aba@fnal.gov

†Electronic address: gfuller@ucsd.edu

nos [15]. Sterile neutrinos with masses of 1 – 100 keV and small mixings with active neutrinos are produced in the non-equilibrium quantum decoherence process associated with the scattering of active neutrinos: either with the usual simplifying assumption of a small universal lepton number [9] (of order the baryon number) or with the more liberal possibility of a large lepton number in neutrinos (several orders of magnitude larger than the baryon number) [11]. We define lepton number in a neutrino flavor here as the difference between neutrino and antineutrino number densities normalized by the photon number density, n_γ , at a given epoch: $L_\alpha \equiv (n_{\nu_\alpha} - n_{\bar{\nu}_\alpha})/n_\gamma$.

Constraints on the lepton numbers which reside in the neutrino seas can be made by requiring successful production of the light element abundances in primordial nucleosynthesis while keeping the baryon density compatible with that inferred from observations of the cosmic microwave anisotropies [16]. Because of the near bi-maximal mixing paradigm emerging for the neutrino mass matrix, more stringent constraints can be placed on neutrino lepton number since asymmetries in the more poorly-constrained mu and tau flavors can be converted to an asymmetry in the more stringently-constrained electron neutrinos through synchronized flavor transformation [17]. However, even the strongest constraint available, on electron neutrino lepton number, allows $|L_e|_{1\text{ MeV}} \lesssim 0.1$ at the epoch of nucleosynthesis. Because sterile neutrinos are produced at temperatures much higher than those characterizing BBN, and because lepton number (unlike degeneracy parameter) is not a comoving invariant, we quote values of lepton number at the epoch where $T = 100$ GeV. Therefore, the most conservative upper bound on lepton number at this temperature is weaker by the ratio of the number of statistical degrees of freedom $g(T)$ in the plasma, $g(100\text{ GeV})/g(1\text{ MeV})$, or $|L_e|_{100\text{ GeV}} \lesssim 1$. All lepton-number driven mechanisms we consider are well within this conservative limit.

Depending on their masses and non-thermal energy distributions, the sterile neutrinos produced in the early universe can be CDM, WDM, or hot dark matter (HDM). The production mechanisms and constraints on these models were studied in Refs. [10, 12]. The strongest constraints on the upper bound of the mass of the sterile neutrino derive from x-ray emission from nearby galaxy clusters, *viz.* the Virgo cluster [18], $m_s \lesssim 5$ keV when $L \sim 10^{-10}$. Lower bounds on the mass of the WDM particle can be made by requiring that its free-streaming not excessively damp out small-scale structure, *i.e.*, behave too much like HDM. Limits of this type come from the observed structure on small scales in the high-redshift Lyman- α forest [19] and by requiring sufficiently early reionization of the universe seen by the Gunn-Peterson effect [20]. A lower bound on the mass can also be derived from the observed phase-space densities of galaxy cores [4]. All of these limits require out-of-equilibrium (“standard”) WDM particles with mass $m \gtrsim 0.75$ keV, or sterile neutrino WDM in models where $L \sim 10^{-10}$

with mass $m_s \gtrsim 2.6$ keV [21]. It is exciting that the currently unconstrained mass range $2.6\text{ keV} \lesssim m_s \lesssim 5\text{ keV}$ (at $L \sim 10^{-10}$), is that favored by WDM solutions to small scale structure formation, and, even more, this mass range for the sterile neutrino dark matter is also eminently detectable via radiative decay [18].

II. THE QUARK-HADRON TRANSITION

The study of the condensed matter physics of QCD remains an active topic, through analysis of the full color $SU(3)$ QCD Lagrangian with numerical lattice simulation and analogy with spin systems (for a recent survey see Ref. [22]). The nature of the QCD transition at finite temperature and zero chemical potential μ_q is clear in models containing two massless quarks ($m_{q_u} = m_{q_d} = 0$, $m_{q_s} \rightarrow \infty$): the transition is second-order [23]. With physically realistic small but nonzero m_{q_u} and m_{q_d} , the second-order transition loses its critical behavior and is a smooth crossover [24]. In degenerate three-flavor models ($m_{q_u} = m_{q_d} = m_{q_s} = 0$), it was inferred analytically that the transition is first-order [23], and this has been supported by lattice studies [25]. Therefore, with $\mu_q \rightarrow 0$ (as is appropriate for the early universe where $\mu_q/T \sim 10^{-8}$) there exists some critical mass $m_{q_s}^c$, below which the transition is first-order. The position of this critical point in temperature, μ_q , and m_{q_s} is still under investigation by lattice simulations and may be probed by relativistic heavy ion collision experiments [24]. Lattice calculations indicate $m_{q_s}^c$ is well below the inferred physical strange quark mass [25, 26], but these results are not conclusive [27]. Since production of sterile neutrinos peaks at $T \sim 130\text{ MeV}(m_s/3\text{ keV})^{1/3}$, and the QCD transition likely occurs from $T_{\text{crit}} = 100 - 200\text{ MeV}$, the effects of the transition on production are unmistakably important.

Convincing theoretical motivation or experimental detection of the critical endpoint as yet does not exist, and so whether the QCD transition in the early universe behaves as condensing water (first-order) or thickening pudding (smooth crossover) remains to be discovered. We argue below how the dark matter, if sterile neutrinos, can also be used to probe the critical behavior of QCD.

We model the evolution of the universe through a first-order transition as in Refs. [28, 29]. The transition from the high-temperature quark-gluon phase to the hadron phase includes the change in the statistical degrees of freedom of the plasma, the release of vacuum energy, and the annihilation of quark-antiquark pairs. Supercooling of the plasma can lead to nucleation of remaining quarks into dense isothermal baryon number fluctuations [30], but this does not affect the analysis here.

A first-order transition evolves through a constant-temperature epoch, with duration of order a Hubble-time at that epoch. During this constant temperature, mixed phase regime, volume is swapped from the quark-gluon phase to bubbles of hadronic phase as the universe ex-

pands. In this scenario the fraction of the volume in the quark-gluon phase evolves from $f_v = 1$ to 0, at which time the transition ends. The two phases differ in entropy density and therefore latent heat is released in the transition. The dynamics of the scale factor, a , through the transition is given by [29, 31]

$$\frac{\dot{a}}{a} = \chi \left(4f_v + \frac{3}{x-1} \right)^{1/2}, \quad (2.1)$$

where $x \equiv g_q/g_h$ is the ratio of the number of relativistic degrees of freedom in the quark g_q and hadron g_h phases (approximately valid during the mixed phase epoch), and the characteristic QCD expansion rate is

$$\chi \equiv \left(\frac{8\pi B}{3m_{\text{Pl}}^2} \right)^{1/2} \approx (143 \mu\text{s})^{-1} \left(\frac{T_{\text{crit}}}{100 \text{ MeV}} \right)^2. \quad (2.2)$$

Here the vacuum energy is parametrized by an effective ‘‘bag constant’’ B . Pressure equilibrium between quark and hadron phases is used to find the relation between the vacuum energy and transition’s critical temperature, T_{crit} .

Using the conservation of comoving entropy it can be shown that the fraction of the plasma in the quark-gluon phase at a given time, t , from the start of the transition at time, t_i , is [29]

$$f_v = \frac{1}{4(x-1)} \left\{ \tan^2 \left[\arctan \left[(4x-1)^{1/2} \right] + \frac{3\chi(t_i-t)}{2(x-1)^{1/2}} \right] - 3 \right\}. \quad (2.3)$$

These relations are used to calculate the cosmological dynamics for sterile neutrino dark matter production during the first-order transition. The evolution of temperature for a first-order and crossover transition is shown in Fig. 1.

III. DARK MATTER PRODUCTION

Production of sterile neutrino dark matter occurs through decoherence of the active neutrino gas via collisions with the background plasma of weakly interacting particles. We calculate this incoherent production of sterile neutrinos as described in Ref. [12], which we summarize here. This incoherent production is described by a semi-classical Boltzmann equation that captures the quantum behavior of the system. The distribution function for sterile neutrinos f_s over momenta p evolves as

$$\begin{aligned} \frac{\partial}{\partial t} f_s(p, t) - H p \frac{\partial}{\partial p} f_s(p, t) \\ = \Gamma(\nu_\alpha \rightarrow \nu_s; p, t) [f_\alpha(p, t) - f_s(p, t)]. \end{aligned} \quad (3.1)$$

Here f_α is the active neutrino distribution function that is coupled to the sterile, $\Gamma(\nu_\alpha \rightarrow \nu_s; p, t)$ is the effective

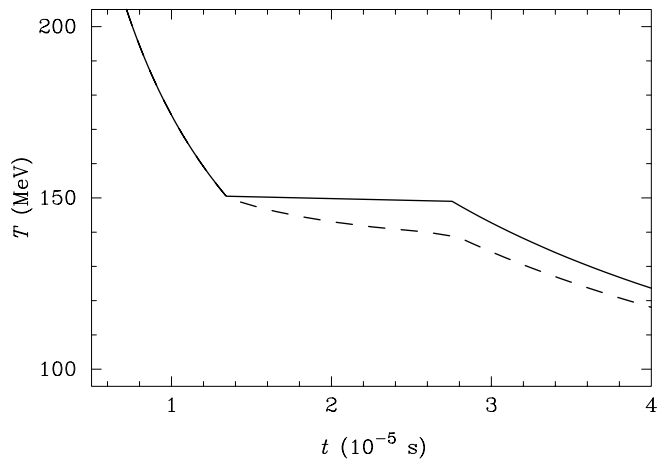


FIG. 1: Evolution of temperature for a first-order transition (solid) and crossover transition (dashed) for $T_{\text{crit}} = 150 \text{ MeV}$.

rate of production (annihilation) of sterile states and $H = \dot{a}/a$.

It is important to note that the scattering kernels $\Gamma(\nu_\alpha \rightarrow \nu_s; p, t)$ for the case of sterile neutrino production are always momentum conserving [32] so that Eq. (3.1) is exact. We handle the calculation of this scattering kernel as described in Ref. [12]. This includes augmenting the scattering rate as the population of weak scatterers increases at high temperatures.

The behavior of the QCD transition affects dark matter production through the varied evolution of the total energy density, ρ_{tot} , of the plasma for different critical behavior. In turn, this modifies the evolution of the expansion rate through the Friedmann equation $H = \sqrt{8\pi/3} m_{\text{Pl}}^{-1} \rho_{\text{tot}}^{1/2}$. The dynamics of expansion enters the calculation of dark matter production in two ways: (1) alteration of the time-temperature relationship; (2) the modification of redshifting of relativistic species, including sterile neutrinos.

If the universe underwent a crossover QCD transition (i.e., no phase transition), the effects on sterile neutrino densities stem entirely from the annihilation of quark-antiquark pairs and the resulting disappearance of degrees of freedom in the plasma. The entropy carried in the annihilating species is transferred to the remaining constituents of the plasma. The time-temperature relation in the early universe with evolving numbers of thermalized species is far from a new problem. This is basically the same effect (though more pronounced) on the time-temperature relation as that caused by the annihilation of electron-positron pairs when $T \sim 25 \text{ keV}$. A general treatment of the time-temperature relationship including the effects of the population of sterile neutrinos is given in the appendix of Ref. [12], whose approach we have incorporated. A crossover transition disturbs production by causing the universe to ‘‘linger’’ for some time at temperatures just below the critical temperature (see Fig. 1). Since the QCD transition temperatures can be at

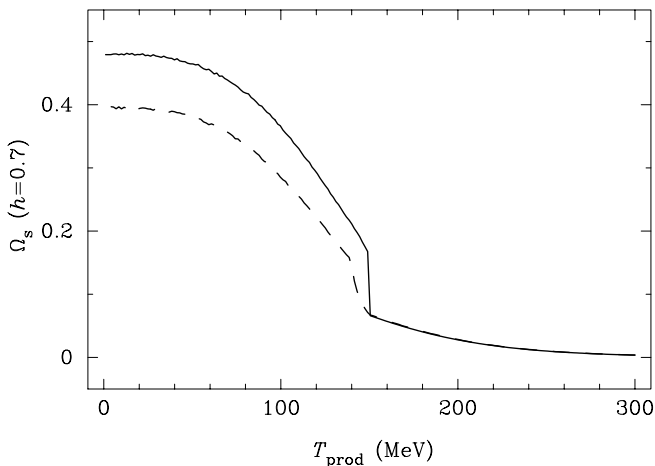


FIG. 2: The fraction of critical density Ω_s produced above a temperature T_{prod} . Here we have taken $T_{\text{crit}} = 150$ MeV. There is significant enhancement due to thermal lingering after T_{crit} for a crossover transition (dashed), and there is a dramatic enhancement at T_{crit} in the first-order case (solid). The most significant difference between the two cases stems from the delay of the radiation-dominated era in a first-order transition. Here we have taken $m_s = 3$ keV, $\sin^2 2\theta = 2.6 \times 10^{-8}$, and $L \sim 10^{-10}$.

or near the peak rate of dark matter production, the position of the post-critical temperature lingering may enhance the production. A representative case of dark matter production through a crossover transition is shown in Fig. 2.

The temperature is constant in a first-order transition, and the duration of the transition is given by the time required for the quark phase to disappear, Eq. 2.3. Here, the production with temperature is a step-like function at the critical temperature as a result of the finite time spent at T_{crit} (see Fig. 2). More significant than the production during the transition is the delay of the radiation domination epoch by a first-order transition, so that the time-temperature relation is modified from the standard case, $t \propto T^{-2}$. The duration of the first order transition can be obtained by Eq. (2.3),

$$\Delta t = \frac{2(x-1)^{1/2}}{3\chi} \left[\arctan \left[4(x-1)^{1/2} \right] - \arctan 3^{1/2} \right], \quad (3.2)$$

which for typical parameters is approximately 2×10^{-5} s. A first-order transition universe will then spend slightly more time reaching a given temperature. This can be seen in Fig. 1. This delay in the temperature decrease with expansion is a major factor in enhancing dark matter production in a first-order transition universe. That is, the partial equilibration of the sterile neutrinos has more time to operate in the first-order case.

The expansion also modifies the redshifting of sterile neutrino momenta ($p \propto a^{-1}$). In a radiation-dominated environment, and with a crossover transition $p \propto t^{-1/2}$. However, during a first-order phase transition the mo-

mentum will scale inversely with the scale factor as found by integrating Eq. (2.1). Handling the redshifting explicitly through these scalings as opposed to using the second term on the left-hand-side of Eq. (3.1) greatly accelerates numerical computation by eliminating the calculation of the momentum derivative of the time-evolving sterile neutrino distribution.

The final effect of the transition we consider is sterile neutrino dilution by the heating of the thermally coupled species in the plasma relative to the uncoupled dark matter by entropy transfer (latent heat release). Exclusive of all other effects in a crossover transition, this produces a heating of the coupled species relative to the dark matter. With the assumption that the crossover transition is rapid relative to the expansion time, the dilution of the dark matter relative to coupled species is given by comoving entropy conservation as $x^{-1} = g_h/g_q \sim 1/3$. A crossover transition does not necessarily take place in less than the expansion timescale, as can be seen for the cases we consider in Fig. 1. Therefore, the dilution should be handled by a Boltzmann formulation as is automatically done in our treatment of Eq. (3.1) and the time-temperature relation. For a crossover transition, dilution is the major factor in determining the different critical density contributions shown in Fig. 3. In a first-order transition, dilution effects are handled in the evolution of the scale factor (2.1) and time-temperature relation.

We have included all of the above effects in a numerical solution of the production equations (3.1). Contours of predicted sterile neutrino critical densities of $\Omega_s h^2 = 0.15$ for three representative lepton number cosmologies and both first-order and crossover QCD transitions are shown in Fig. 4. The shape of the large lepton number cosmology contours can be understood from the resonance condition for a neutrino of momentum p :

$$\begin{aligned} \frac{p}{T} \Big|_{\text{res}} &= \frac{\delta m^2 \cos 2\theta}{8\sqrt{2}\zeta(3)G_F L_\alpha T^4/\pi^2} \\ &\approx 0.3 \left(\frac{m_s}{1 \text{ keV}} \right)^2 \left(\frac{0.01}{L_\alpha} \right) \left(\frac{150 \text{ MeV}}{T} \right)^4. \end{aligned} \quad (3.3)$$

The largest disparity between first order and crossover transitions occurs when the resonance position is in a populated portion of the neutrino momentum distribution (of order $p/T \sim 1$) at T_{crit} . For an $L = 0.01$ cosmology, the resonance is in the peak of the momentum distribution at T_{crit} for masses $m_s \approx 13$ keV, the pronounced effects of the nature of the transition for this case can be seen in Fig. 4. Furthermore, for this lepton number, the resonance position falls at very low momenta for $m_s < 1$ keV during the peak production. Therefore, production is thermally suppressed, leading to the break seen at $m_s \sim 1$ keV for $L = 0.01$ cosmologies in Fig. 4.

An effect present in above the quark-hadron transition is that of quark screening, or many-body neutrino-quark scattering. The mean distance between quarks above the quark-hadron transition at $T \sim 150$ MeV is approximately $l \sim (3\zeta(3)g_q/\pi^2)^{-1/3}T^{-1} \sim 1$ fm,

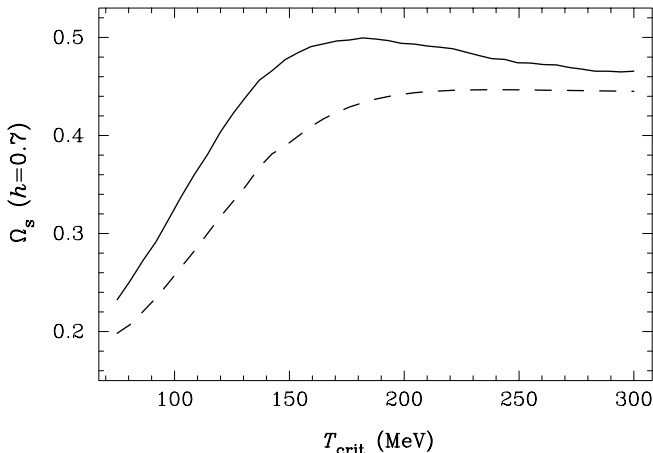


FIG. 3: Critical density for a varying critical temperature for the QCD transition. Solid line is for a simple crossover QCD transition; dashed line is for a first order transition. Here we have specified $m_s = 3$ keV, $\sin^2 2\theta = 2.6 \times 10^{-8}$, and $L \sim 10^{-10}$.

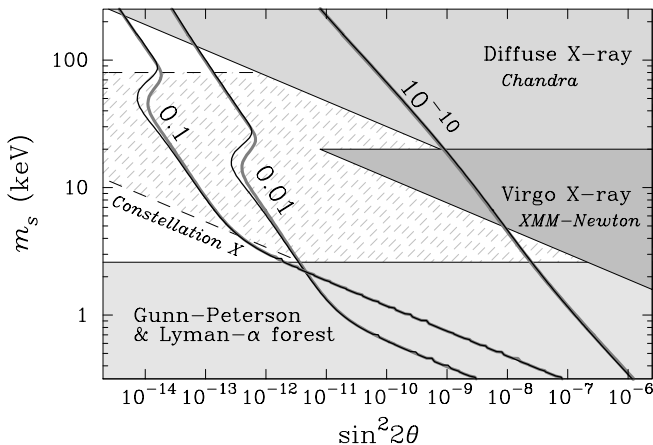


FIG. 4: Shown is the parameter space available for sterile neutrino dark matter, with varying lepton-number cosmologies. The contours (numbered by their initial lepton number) are positions in the mass and mixing angle space where sterile neutrinos produce critical densities of $\Omega_s h^2 = 0.15$. The thin (thick) lines are for a first-order (crossover) QCD transitions ($T_{\text{crit}} = 150$ MeV). Also shown are the excluded regions (shaded gray) from small scale structure—the Gunn-Peterson bound and Lyman- α forest—and halo phase space densities, the resolution of the diffuse X-ray background by *Chandra*, and observations of the Virgo cluster by *XMM-Newton*. The dashed region is that which may be probed by the proposed *Constellation-X* mission [18].

and the de Broglie wavelength of a typical neutrino is $\lambda \sim \hbar/p \sim 0.4$ fm. Therefore, neutrinos below the average momentum will have $\lambda > l$, and two-body scattering is no longer well-defined. Many-body scattering will tend to cancel the weak charge of quarks and antiquarks, and reduce the effectiveness of decohering interactions of active neutrinos. The effects of many-body scattering are

beyond the scope of this work. Though it can be significant in altering scattering rates above the QCD transition, the majority of sterile neutrino dark matter is produced below the QCD transition (as seen in Fig. 2) and the resulting effects of quark screening will be relatively small.

IV. PROBING THE QCD TRANSITION WITH DARK MATTER

In order to predict the sterile neutrino dark matter density one must specify the singlet neutrino rest mass m_s , vacuum mixing with active neutrinos $\sin^2 2\theta$, the initial lepton number L , and the order of the QCD transition and its critical temperature T_{crit} . Since the dark matter density is being determined rather precisely [33], the sterile neutrino production mechanism will constrain the relationship between the sterile neutrino properties and parameters describing the background plasma.

It was shown in Ref. [18] that the radiative decay of sterile neutrino dark matter $\nu_s \rightarrow \nu_\alpha \gamma$ may be detected with high-sensitivity spectrographs aboard the current *Chandra* or *XMM-Newton* X-ray telescopes, or with the proposed large-surface-area and precision spectrograph of the *Constellation X* mission. As noted earlier, the lack of a significant line in the observation of the Virgo cluster constrains the largest possible mass of a sterile neutrino dark matter candidate produced in the zero-lepton-number case ($m_s \lesssim 5$ keV). This constraint comes from the fact that the Virgo cluster is one of the better candidate objects [18] and a high-sensitivity spectrum is available [34]. Observations of this and other clusters and field galaxies with current X-ray observatories can either detect or exclude sterile neutrino dark matter as a dark matter candidate in zero-lepton-number universes.

If sterile neutrinos are the dark matter, detection of radiative decay by a sufficiently sensitive observatory would readily identify m_s since the radiative decay produces monoenergetic photons with energy $E_\gamma = m_s/2$. Detection of these photons in the X-ray is most likely in long-duration exposures of nearby high surface dark matter mass density objects. The X-ray flux coming from radiative decay of a sterile neutrino is

$$F \approx 5.1 \times 10^{-18} \text{ erg cm}^{-2} \text{ s}^{-1} \left(\frac{D}{\text{Mpc}} \right)^{-2} \left(\frac{M_{\text{DM}}}{10^{11} M_\odot} \right) \times \left(\frac{\sin^2 2\theta}{10^{-10}} \right) \left(\frac{m_s}{1 \text{ keV}} \right)^5. \quad (4.1)$$

Note that the radiative decay rate of a heavy sterile neutrino is greatly enhanced due to the lack of the GIM-suppression present in the decay of active neutrinos of the same mass and mixing [35].

Since the position of the X-ray line will specify m_s , the strength of the line determines $\sin^2 2\theta$, and therefore the position in Fig. 4. Of the remaining parameters (L_α , T_{crit} and the order of the transition), only a small range

will successfully produce the observed critical density and detected radiative decay flux. However, there remains a degeneracy between L_α and the order of the transition since both a first order transition and a slightly larger L_α can enhance production at smaller mixing angles (see Fig. 4). However, if one can independently determine either the order of the transition or L_α , then the observed flux [Eq. (4.1)] will determine the remaining degree of freedom.

V. CONCLUSIONS

We have presented the results of the most detailed analysis of sterile neutrino dark matter production yet performed. In doing so, we have explored the implications of an unexpected coincidence: the peak production epoch for sterile neutrino dark matter can be the same as the QCD epoch where the quark and gluon degrees of freedom disappear and give way to color singlets. The effects of the QCD transition on sterile neutrino relic densities are bracketed by simple crossovers (no phase transition) and first order phase transitions for the re-ordering of the strongly interacting degrees of freedom from quarks and gluons to hadrons.

We find that the varying alteration in the expansion dynamics in these different models of the QCD transition at high temperature and low chemical potential can give rise to an appreciable range of closure contributions associated with a given singlet sterile neutrino mass, vacuum mixing with active species, and primordial lepton number(s). In particular, first-order phase transition scenarios for the cosmic QCD epoch produce a constant tem-

perature interval with duration of order the Hubble time associated with phase coexistence. This can result in a significant enhancement of sterile neutrino relic densities relative to simple crossover transitions.

Ultimately, we have pointed out here an unexpected connection between strong-interaction scale physics in the early universe on the one hand and low energy scale dark matter relic physics at the present epoch on the other. Whether this connection could someday be exploited to produce insights into the cosmic QCD epoch would, of course, depend on identification of a significant component of the dark matter as being carried by sterile neutrinos.

An accurate calculation of the sterile neutrino production entails following the evolution of the active neutrino scatterer number densities, sterile neutrino production, and entropy transfer-induced dilution for a range of possible behaviors for the strongly strongly interacting sector. Including these effects, we have presented the most sophisticated calculation of the predictions of sterile neutrino relic densities for a range of possible QCD transition scenarios and lepton number cosmologies.

Acknowledgments

We would like to thank John Beacom, Nicole Bell, Steen Hansen and Rocky Kolb for useful discussions, and, in addition, thank Rocky Kolb for providing a rapid numerical calculator of the evolution of the number of statistical degrees of freedom in the early universe. This research was supported in part by the DOE and NASA grant NAG 5-10842 at Fermilab and by NSF Grant PHY00-99499 at UCSD.

-
- [1] M. S. Turner, *Phys. Rept.* **333**, 619 (2000);
X. Wang, M. Tegmark, and M. Zaldarriaga, *astro-ph/0105091*;
N. A. Bahcall, J. P. Ostriker, S. Perlmutter, and P. J. Steinhardt, *Science* **284**, 1481 (1999), [[arXiv:astro-ph/9906463](#)].
 - [2] B. Moore *et al.*, *Astrophys. J. Lett.* **524**, L19 (1999).
 - [3] S. Ghigna *et al.*, *Astrophys. J.* **544**, 616 (2000).
 - [4] J. J. Dalcanton and C. J. Hogan, *Astrophys. J.* **561**, 35 (2001).
 - [5] J. S. Bullock, A. V. Kravtsov, and D. H. Weinberg, *Astrophys. J.* **548**, 33 (2001).
 - [6] S. Colombi, S. Dodelson, and L. M. Widrow, *Astrophys. J.* **458**, 1 (1996);
P. Colin, V. Avila-Reese, and O. Valenzuela, *Astrophys. J.* **542**, 622 (2000);
P. Bode, J. P. Ostriker, and N. Turok, *Astrophys. J.* **556**, 93 (2001).
 - [7] N. Dalal and C. S. Kochanek, [arXiv:astro-ph/0202290](#).
 - [8] V. Avila-Reese, P. Colin, O. Valenzuela, E. D'Onghia, and C. Firmani, *Astrophys. J.* **559**, 516 (2001).
 - [9] S. Dodelson and L. M. Widrow, *Phys. Rev. Lett.* **72**, 17 (1994), [hep-ph/9303287](#).
 - [10] A. D. Dolgov and S. H. Hansen, *Astropart. Phys.* **16**, 339 (2002).
 - [11] X. Shi and G. M. Fuller, *Phys. Rev. Lett.* **82**, 2832 (1999).
 - [12] K. Abazajian, G. M. Fuller, and M. Patel, *Phys. Rev. D* **64**, 023501 (2001).
 - [13] N. Arkani-Hamed and Y. Grossman, *Phys. Lett. B* **459**, 179 (1999).
 - [14] Z. G. Berezhiani and R. N. Mohapatra, *Phys. Rev. D* **52**, 6607 (1995).
 - [15] E. J. Chun and H. B. Kim, *Phys. Rev. D* **60**, 095006 (1999).
 - [16] J. P. Kneller, R. J. Scherrer, G. Steigman and T. P. Walker, *Phys. Rev. D* **64**, 123506 (2001);
S. H. Hansen, G. Mangano, A. Melchiorri, G. Miele and O. Pisanti, *Phys. Rev. D* **65**, 023511 (2002);
M. Orito, T. Kajino, G. J. Mathews and Y. Wang, [arXiv:astro-ph/0203352](#).
 - [17] A. D. Dolgov, S. H. Hansen, S. Pastor, S. T. Petcov, G. G. Raffelt and D. V. Semikoz, [arXiv:hep-ph/0201287](#);
K. N. Abazajian, J. F. Beacom and N. F. Bell, [arXiv:astro-ph/0203442](#);
Y. Y. Wong, [arXiv:hep-ph/0203180](#).

- [18] K. Abazajian, G. M. Fuller and W. H. Tucker, *Astrophys. J.* **562**, 593 (2001).
- [19] V. K. Narayanan, D. N. Spergel, R. Davé, and C. Ma, *Astrophys. J. Lett.* **543**, L103 (2000).
- [20] R. Barkana, Z. Haiman and J. P. Ostriker, *Astrophys. J.* **558**, 482 (2001).
- [21] S. H. Hansen, J. Lesgourgues, S. Pastor, and J. Silk, (2001), arXiv:astro-ph/0106108.
- [22] H. Satz, *Nucl. Phys.* **A681**, 3 (2001).
- [23] R. D. Pisarski and F. Wilczek, *Phys. Rev.* **D29**, 338 (1984).
- [24] B. Berdnikov and K. Rajagopal, *Phys. Rev.* **D61**, 105017 (2000).
- [25] F. R. Brown *et al.*, *Phys. Rev. Lett.* **65**, 2491 (1990).
- [26] F. Karsch, E. Laermann, and C. Schmidt, *Phys. Lett.* **B520**, 41 (2001).
- [27] Y. Iwasaki, K. Kanaya, S. Kaya, S. Sakai, and T. Yoshie, *Phys. Rev.* **D54**, 7010 (1996).
- [28] C. Alcock, G. M. Fuller, and G. J. Mathews, *Astrophys. J.* **320**, 439 (1987).
- [29] G. M. Fuller, G. J. Mathews, and C. R. Alcock, *Phys. Rev.* **D37**, 1380 (1988).
- [30] E. Witten, *Phys. Rev.* **D30**, 272 (1984).
- [31] K. Kajantie and H. Kurki-Suonio, *Phys. Rev.* **D34**, 1719 (1986).
- [32] B. H. J. McKellar and M. J. Thomson, *Phys. Rev. D* **49**, 2710 (1994);
N. F. Bell, R. R. Volkas and Y. Y. Y. Wong, *Phys. Rev. D* **59**, 113001 (1999).
- [33] C. Pryke, N. W. Halverson, E. M. Leitch, J. Kovac, J. E. Carlstrom, W. L. Holzapfel and M. Dragovan, arXiv:astro-ph/0104490;
P. de Bernardis *et al.*, arXiv:astro-ph/0105296.
- [34] H. Böhringer, *et al.*, *Astron. Astrophys.* **365**, L181 (2001).
- [35] P. B. Pal and L. Wolfenstein, *Phys. Rev. D* **25**, 766 (1982).